Local magnetic susceptibility, spin dynamics, and charge order in the quasi-one-dimensional conductor β-$Li_{0.33}V_2O_5$ investigated by site-selective ^{51}V NMR

Ichihiro Yamauchi,[1,*] Masayuki Itoh,[1] Touru Yamauchi,[2] Jun-Ichi Yamaura,[3] and Yutaka Ueda[4]

[1]*Department of Physics, Graduate School of Science, Nagoya University, Furo-cho, Chikusa-ku, Nagoya 464-8602, Japan*

[2]*Institute for Solid State Physics, University of Tokyo, Kashiwa, Chiba 277-8581, Japan*

[3]*Materials Research Center for Element Strategy, Tokyo Institute of Technology, Yokohama, Kanagawa 226-8503, Japan*

[4]*Toyota Physical and Chemical Research Institute, 41-1 Yokomichi, Nagakute, Aichi 480-1192, Japan*

(Received 5 July 2017; revised manuscript received 16 October 2017; published 9 November 2017)

^{51}V NMR measurements have been conducted on a single crystal of the quasi-one-dimensional conductor β-$Li_{0.33}V_2O_5$ which undergoes a metal-insulator (MI) transition at $T_{MI} \sim 170$ K. In the metallic phase, we obtain ^{51}V Knight shift and electric field gradient tensors. From the analysis of the ^{51}V Knight shifts, we find that the charge disproportionation appears even in the metallic state and the electronic structure is represented within a model of weakly coupled ladders containing two types of ladders with distinct carrier densities. Based on the ^{51}V nuclear spin-lattice relaxation rate, we discuss the spin dynamics within the one-dimensional electron gas model. From the analysis of several nonmagnetic V^{5+} spectra observed in the insulating phase, we propose a possible charge-order pattern which has a superlattice modulation larger than those in other family members of β-$A_{0.33}V_2O_5$ (A = Na and Ag). Finally, we discuss the A-ion dependence of the electronic structure, the charge disproportionation, and the charge order in β-$A_{0.33}V_2O_5$.

DOI: 10.1103/PhysRevB.96.205114

I. INTRODUCTION

Searching for a new ordered state of spin, charge, and orbital degrees of freedom is one of the central issues in condensed matter physics. Such an ordered state is fascinating not only as a new phase of material but also as a mother phase with anomalous metallic behaviors, for instance, colossal magnetoresistance and high-temperature superconductivity [1]. These phenomena appear in the vicinity of the ordered state, and the orderings and fluctuations of the above degrees of freedom are a key to understand the mechanism of the physical properties. Ternary 3d transition-metal oxides are regarded as one of the playground for such exotic states due to low dimensionality and the mixed valence of the transition-metal ions. Recently, various exotic phenomena have been discovered in quasi-one-dimensional (quasi-1D) oxides with hollandite and calcium-ferrite-type structures such as a metal-insulator (MI) transition accompanied by charge ordering (CO), an MI transition in a ferromagnetic phase, and colossal magnetoresistance in an antiferromagnetic phase [2–12]. Another quasi-1D metallic system is β-$A_{0.33}V_2O_5$ (A = Li, Na, and Ag) which have been extensively investigated as a highlight material of the ternary vanadium oxides.

β-$A_{0.33}V_2O_5$, which have a nominal mixed valence of $V^{4+}(3d^1)$ and $V^{5+}(3d^0)$ as $V^{4+}:V^{5+}=1:5$, commonly show an MI transition at T_{MI} = 90–170 K accompanied by CO [13–15]. An antiferromagnetic transition takes place well below T_{MI} [13–19] at ambient pressure and a superconducting phase appears at 7–10 GPa above which the MI transition is suppressed [15,20–25]. As shown in Fig. 1, β-$A_{0.33}V_2O_5$ fundamentally crystallize in a monoclinic structure and have three crystallographically inequivalent vanadium sites V1, V2, and V3. Each V site is surrounded by O^{2-} anions with the octahedral (V1, V2) or pyramidal (V3) coordination and these polyhedra form infinite chains along the b axis [26]. The cation site is located in a tunnel formed by the V_2O_5 framework and only a half of the site is occupied by the A ion in the β-type structure. The A ion shows a zigzag ordering with the $a \times 2b \times c$ superlattice structure. This ordering changes the space group from $C2/m$ to $P2_1/a$ and splits the VS (S = 1–3) site into two inequivalent sites, VSA and VSB [19,27]. For instance, the zigzag ordering transition occurs at T_A = 242 and 200 K for the A = Na and Ag systems, respectively. Furthermore, the $a \times 6b \times c$ superlattice structure with the space group $P2_1/a$ was confirmed in the CO state except the A = Li system [19,27–29].

Among the intriguing phenomena mentioned above, the CO pattern and the mechanism of its formation have attracted much attention as a fundamental issue in β-$A_{0.33}V_2O_5$. The CO pattern has been intensively investigated for β-$A_{0.33}V_2O_5$ (A = Na and Ag), whereas it has not been clarified for the A = Li system [18,19,27,30–34]. The CO pattern is considered to be governed by the electron filling, hopping energy, and Coulomb interaction in many cases. However, the proposed CO models for the A = Na and Ag systems are different from each other, although both systems have the same electron filling. Furthermore, it has been suggested that the charge density at each V site is modified by the zigzag ordering of the A ion even in the metallic state, which is abbreviated to charge disproportionation (CD) hereafter [35,36]. These facts indicate that the A ion also provides a different effect on the CD and CO patterns in β-$A_{0.33}V_2O_5$. Thus, an NMR experiment on β-$Li_{0.33}V_2O_5$ is useful to systematically understand the A dependence of the CD and CO patterns.

Previously, we reported ^{7}Li NMR results on a single crystal of β-$Li_{0.33}V_2O_5$ [37,38]. We observed two sets of ^{7}Li NMR spectra suggesting the presence of two crystallographically inequivalent Li sites in the metallic phase. The angular dependence of the ^{7}Li NMR spectra clearly showed the

*Present address: Department of Physics, Graduate School of Science and Engineering, Saga University, 1 Honjo-cho, Saga 840-8502, Japan; ichihiro@cc.saga-u.ac.jp

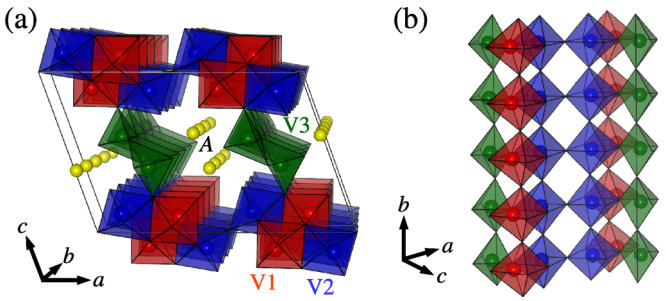

FIG. 1. (a) Crystal structure of β-$A_{0.33}V_2O_5$. (b) Basic unit of the electronic structure composed of two V1-V3 ladders and one V2-V2 ladder.

existence of the Li zigzag ordering even at 300 K. Furthermore, an additional $2a$ modulation was pointed out by an x-ray diffraction study [39]. These results indicate a unique structure of β-$Li_{0.33}V_2O_5$ that the $2a \times 2b \times c$ superlattice modulation, which does not appear in the other β-$A_{0.33}V_2O_5$ systems, takes place due to the Li ordering in the metallic phase. However, we could not obtain any information on the CD and CO patterns.

In this paper, we have made ^{51}V NMR measurements on a single crystal to elucidate local magnetic properties, spin dynamics, and charge order in β-$Li_{0.33}V_2O_5$. From the data of the Knight shift, we obtain local spin susceptibility at each V site showing the presence of CD in the metallic state. Spin dynamics is also discussed from the analysis of the nuclear spin-lattice relaxation rate within the 1D electron gas model. Broad and complicated NMR spectra due to the formation of the CO are observed in the insulating phase. Based on the present NMR results, we propose possible CD and CO patterns. Common and different characteristics in the electronic structure, the CD pattern, and the CO pattern are discussed for β-$A_{0.33}V_2O_5$ (A = Li, Na, and Ag).

II. EXPERIMENTAL PROCEDURE

As-grown β-$Li_xV_2O_5$ single crystals, which have excess Li content above the stoichiometric concentration $x = 0.33$, were grown in N_2 atmosphere by the rf-heating Czochralski method using $LiVO_3$ as a flux in a Pt crucible. A stoichiometric single crystal was obtained by calcination of a single crystal with a large amount of $x = 0.33$ powder samples in an evacuated quartz tube at 600 °C for 20 h [20,24]. We confirmed that the single crystal undergoes an MI transition at 170 K.

Fourier-transformed (FT) ^{51}V NMR spectra of spin-echo signals were obtained with the sample rotated in a magnetic field of $H_0 = 5.8709$ T. The field direction is defined by θ_α ($\alpha = c$, a^*, and b) where θ_c is the angle from the a^* axis perpendicular to both the b and c axes in the a^*b plane, whereas the other angles are defined by cyclic permutation of c, a^*, and b. The ^{51}V Knight shift K was determined by using a relation $K = (\nu_{res} - \nu_0)/\nu_0$ where ν_{res} and ν_0(=65.706 MHz) are ^{51}V resonance frequencies in β-$Li_{0.33}V_2O_5$ and aqueous $NaVO_3$, respectively. The ^{51}V nuclear spin-lattice relaxation rate $1/T_1$ was measured by the inversion recovery method with H_0 parallel to a magic angle where the quadrupole splitting vanishes. Then, the nuclear magnetization was observed to recover exponentially with a time constant T_1.

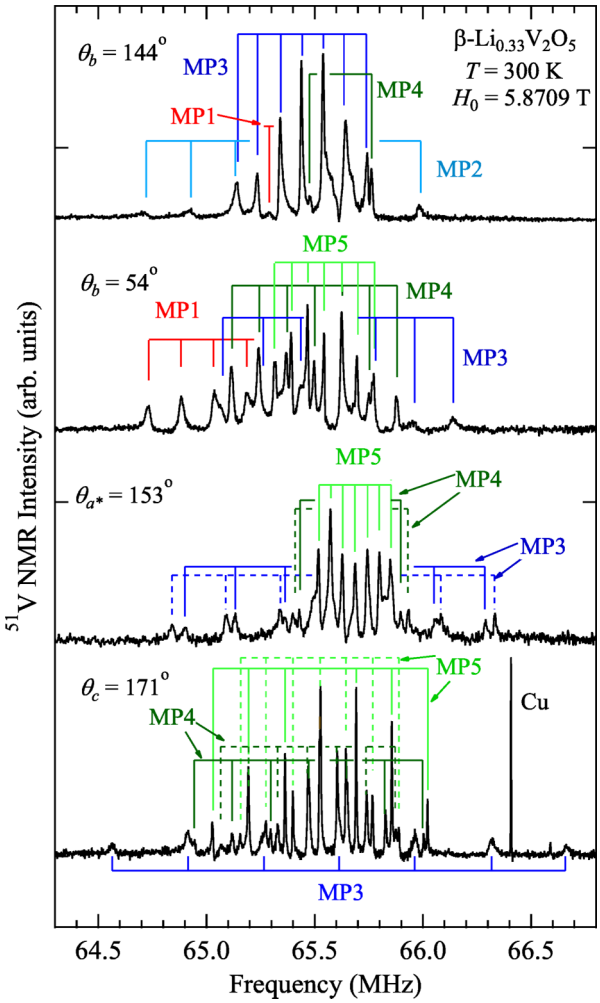

FIG. 2. ^{51}V NMR spectra at 300 K with $H_0 = 5.8709$ T applied along the $\theta_b = 144°$, 54°, $\theta_{a^*} = 153°$, and $\theta_c = 171°$ in a single crystal of β-$Li_{0.33}V_2O_5$. Solid and dotted lines represent ^{51}V spectra, MP1, MP2, MP3, MP4, and MP5, split by the electric quadrupole interactions. The symbol Cu is a ^{63}Cu NMR spectrum coming from a Cu coil.

III. EXPERIMENTAL RESULTS AND ANALYSIS

A. Metallic phase

1. NMR spectrum and Knight shift

Figure 2 displays typical ^{51}V (nuclear spin $^{51}I = \frac{7}{2}$) NMR spectra which are composed of five spectra MP1, MP2, MP3, MP4, and MP5 with H_0 parallel to $\theta_b = 54°$, 144°, $\theta_{a^*} = 153°$, and $\theta_c = 171°$ at 300 K in the metallic phase (MP) of β-$Li_{0.33}V_2O_5$. Each spectrum of MP1–MP5 has equally spaced seven lines, one central and six satellite lines, split by the first-order electric quadrupole effect. The angular dependencies of the ^{51}V NMR frequency and K with H_0 rotated around the c, a^*, and b axes at 300 K are plotted in Figs. 3 and 4, respectively. The experimental data of the angular dependence of the difference between resonance frequencies of the $m \leftrightarrow m-1$ and $-(m-1) \leftrightarrow -m$, ($m = -I+1, \ldots, +I$), satellite lines, $\delta\nu_{m\leftrightarrow m-1}$, for the H_0 rotation around the a^* axis (the a^* rotation) were well fitted by the

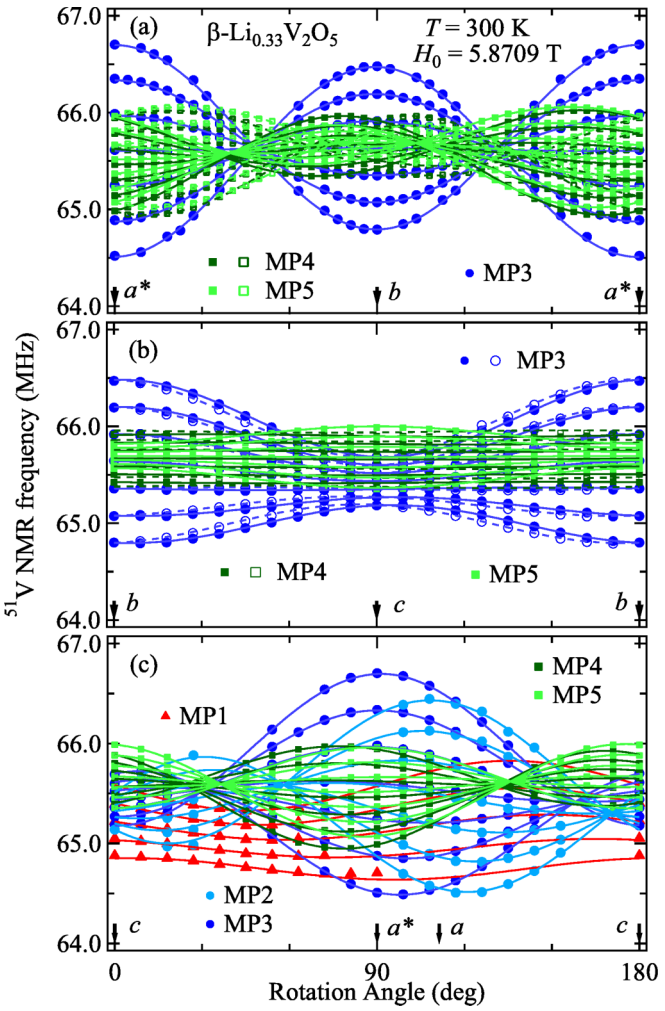

FIG. 3. Angular dependence of the ^{51}V NMR frequency of the MP1, MP2, MP3, MP4, and MP5 spectra at 300 K with $H_0 = 5.8709$ T rotated in the (a) a^*b, (b) bc, and (c) ca^* planes of β-$Li_{0.33}V_2O_5$. Solid and dashed curves are the calculated results using the relation $\nu = \delta\nu_{m\leftrightarrow m-1}/2 + (1+K)\nu_0$ and the fitted EFG and K values listed in Table I.

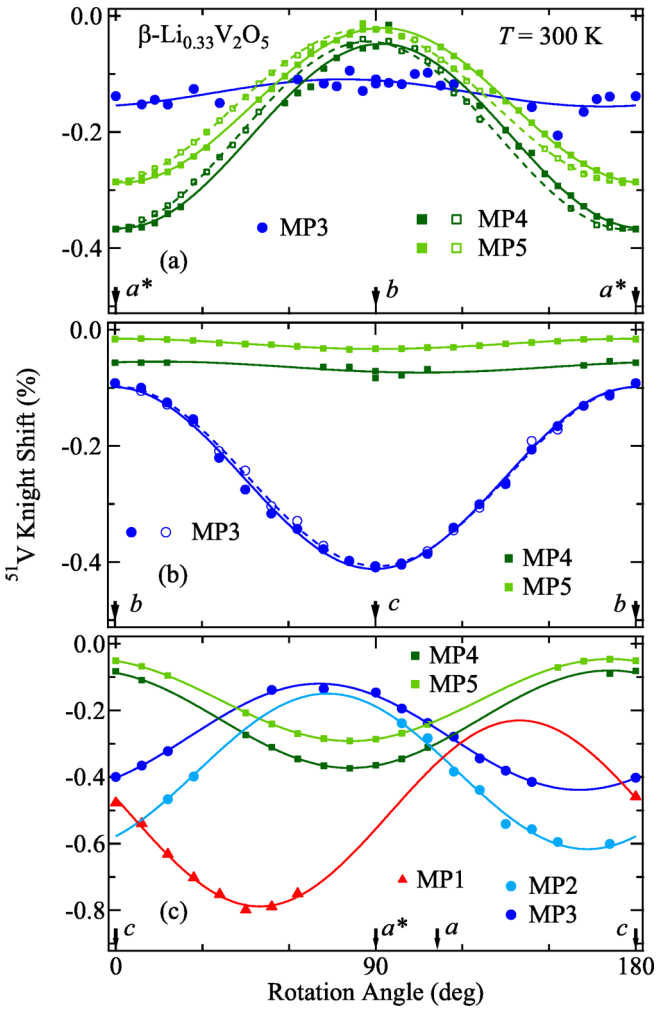

FIG. 4. Angular dependence of the ^{51}V Knight shift of the MP1, MP2, MP3, MP4, and MP5 spectra at 300 K with $H_0 = 5.8709$ T rotated in the (a) a^*b, (b) bc, and (c) ca^* planes of β-$Li_{0.33}V_2O_5$. Solid and dashed curves are the results of fitting the data to Eq. (2).

equation [31,40]

$$\delta\nu_{m\leftrightarrow m-1} = \left(m - \tfrac{1}{2}\right)(\nu_{1,a^*} + \nu_{2,a^*}\cos 2\theta_{a^*} + \nu_{3,a^*}\sin 2\theta_{a^*}), \tag{1}$$

with

$$\nu_{1,a^*} = \nu_Q(V_{bb} + V_{cc})/V_{zz},$$
$$\nu_{2,a^*} = \nu_Q(V_{bb} - V_{cc})/V_{zz},$$
$$\nu_{3,a^*} = -2\nu_Q V_{bc}/V_{zz},$$

and

$$\nu_Q = \frac{3eQV_{zz}}{2I(2I-1)h},$$

where $V_{\alpha\beta}$ ($\alpha,\beta = a^*,b,c$) is the electric field gradient (EFG) tensor described in the a^*bc coordinated system, V_{zz} is the maximum component ($|V_{xx}| \leqslant |V_{yy}| \leqslant |V_{zz}|$) of the EFG tensor in the principal coordinate system $V_{\gamma\gamma}$ ($\gamma = x,y,z$), e is the elementary charge, Q is the nuclear quadrupole moment, and h is the Planck's constant. The equations for the other two rotations are obtained by cyclic permutation of a^*, b, and c. Diagonalization of the EFG tensor in the a^*bc system provides the experimental values of the nuclear quadrupole frequency ν_Q, the asymmetry parameter of EFG, $\eta = |V_{xx} - V_{yy}|/|V_{zz}|$, and the direction of the z principal axis z_Q projected on the ca^* plane are listed in Table I. On the other hand, we fitted the data of the angular dependence of K for the a^* rotation to the equation [32]

$$K = k_{1,a^*} + k_{2,a^*}\cos 2\theta_{a^*} + k_{3,a^*}\sin 2\theta_{a^*}, \tag{2}$$

with

$$k_{1,a^*} = (K_{bb} + K_{cc})/2,$$
$$k_{2,a^*} = (K_{bb} - K_{cc})/2,$$
$$k_{3,a^*} = K_{bc},$$

where $K_{\alpha\beta}$ ($\alpha, \beta = a^*, b, c$) are components of the K tensor in the a^*bc system. The similar equations are obtained for the other rotations by cyclic permutation of a^*, b, and c. By diagonalizing the tensor, we could obtain the principal values

TABLE I. Principal components of the ^{51}V Knight shift K_x, K_y, and K_z, the electric quadrupole frequency ν_Q, the asymmetry parameter of EFG η, and directions of principal axes of the K and EFG tensors z_K and z_Q projected on the ca^* plane for the MP1, MP2, MP3, MP4, and MP5 spectra at 300 K in β-$Li_{0.33}V_2O_5$. The MP1–MP5 spectra are considered to come from the V1B$^{(j)}$, V2A$^{(j)}$, V2B$^{(j)}$, V3A$^{(j)}$, and V3B$^{(j)}$ (j = 1–n) sites, respectively (see text). One possible crystal structure with $2a \times 2b \times c$ unit cell, the monoclinic structure with the space group of $P2_1$, has $n = 4$ as presented in Fig. 13(d).

Spectrum	V site	K_x (%)	K_y (%)	K_z (%)	z_K [θ_b (°)]	ν_Q (MHz)	η	z_Q [θ_b (°)]
MP1	V1B$^{(1)}$–V1B$^{(n)}$	−0.230		−0.780	50	0.416	0.346	∼b
MP2	V2A$^{(1)}$–V2A$^{(n)}$	−0.150		−0.601	163	0.314	0.051	115
MP3	V2B$^{(1)}$–V2B$^{(n)}$	−0.101	−0.124	−0.444	161	0.367	0.528	94
MP4	V3A$^{(1)}$–V3A$^{(n)}$	−0.050	−0.074	−0.374	81	0.189	0.185	79
MP5	V3B$^{(1)}$–V3B$^{(n)}$	−0.018	−0.037	−0.293	81	0.172	0.245	87

of the K tensor, K_x, K_y, and K_z, and the direction of the z principal axis z_K as listed in Table I.

The site assignment of the observed NMR spectra is based on the principal axis of the K tensor governed by the local symmetry for the crystal structure (space group $C2/m$) with no lattice modulation because the A-cation order does not lead to a drastic change in the K tensor [31]. That is, the z_K axes of the V1 and V3 sites approximately lie in the bc plane, whereas that of the V2 site is in the a^*b plane, as discussed on β-$Na_{0.33}V_2O_5$. Thus, we can conclude that the MP1, "MP2 and MP3," and "MP4 and MP5" spectra come from the V1, V2, and V3 sites, respectively. As seen in Fig. 3, the angular dependencies of the ^{51}V NMR frequency are well traced by the curves calculated using the fitted EFG and the K values.

As mentioned above, we observed two sets of ^{51}V spectra from each VS site except V1, although another set of spectra from the V1 site may be not observed due to the short nuclear spin-spin relaxation time T_2. The $2a \times 2b \times c$ lattice modulation suggested by the x-ray diffraction [39] is expected to split each of the VS (S = 1–3) sites into several crystallographically inequivalent sites. First, the $2b$ modulation naturally results in the appearance of the two inequivalent VSA and VSB sites due to the Li zigzag ordering as discussed in the A-ordered phase of β-$Na_{0.33}V_2O_5$ [36] and β-$Sr_{0.33}V_2O_5$ [35].

Second, the $2a$ modulation is expected to furthermore split each of the VSA and VSB sites into several crystallographically inequivalent sites, VSA$^{(1)}$–VSA$^{(n)}$ and VSB$^{(1)}$–VSB$^{(n)}$, where $n \leqslant 8$ for any space group within the $2a \times 2b \times c$ unit cell. In our previous ^{7}Li NMR measurement, we observed clear splittings of ^{7}Li spectra suggesting the $2a$ modulation [37]. However, the splitting is too small to be detected in the ^{51}V NMR spectra. Therefore, the observed spectra MP1, MP2, MP3, MP4, and MP5 have to come from the V1B$^{(1)}$–V1B$^{(n)}$, V2A$^{(1)}$–V2A$^{(n)}$, V2B$^{(1)}$–V2B$^{(n)}$, V3A$^{(1)}$–V3A$^{(n)}$, and V3B$^{(1)}$–V3B$^{(n)}$ sites, respectively, in the crystal structure with the $2a \times 2b \times c$ modulation. This means that the local magnetic and electric properties of the n crystallographically inequivalent V$X^{(j)}$ sites are so similar that they lead to no splitting in each of the MP1–MP5 spectra. This site assignment of the NMR spectra due to the $2a$ modulation was not discussed in the preliminary report [38].

Another splitting is observed as represented by the solid and dashed lines in Fig. 2 and by the solid symbols with solid curves and the open symbols with dashed curves in Figs. 3 and 4 for the MP3, MP4, and MP5 spectra. This splitting is ascribed to their local symmetry. Even the NMR spectrum from one crystallographically equivalent site is split into two spectra in a magnetic field, if it has the local symmetry providing two types of principal axes in the K and EFG tensors. Figure 5 shows all the V3A$^{(1)}$–V3A$^{(4)}$ and V3B$^{(1)}$–V3B$^{(4)}$ sites in the possible crystal structure with the $P2_1$ space group discussed in Sec. IV B. In this crystal structure, there are two atomic positions for each V3 site which are related with the twofold screw axis. The direction of the principal axes of the K and EFG tensors at the two nuclei sites is different, although the two principal axes are connected to each other with the twofold screw rotation. For instance, one of the principal axes of the EFG tensor y_Q for the V3A$^{(1)}$ site is depicted in Fig. 5. This makes the two angular dependencies of the NMR frequency denoted by solid and dashed curves in Figs. 3(a) and 3(b). Similar splittings were also observed in the NMR spectra of β-$Na_{0.33}V_2O_5$ [31,32].

Finally, we present the T dependencies of the isotropic Knight shift $K_{iso} = (K_x + K_y + K_z)/3$ and the axially anisotropic one $K_{ax} = (2K_z - K_x - K_y)/6$ for the MP1–MP5 spectra in Figs. 6(a) and 6(b), respectively. Then, K_{iso} and K_{ax} are evaluated by assuming the uniaxial anisotropy $K_x = K_y$ for MP1 and MP2. The MP1 spectrum coming from the V1B$^{(j)}$ sites has the largest absolute value of K, whereas the MP5 spectrum from the V3B$^{(j)}$ sites has the smallest value.

2. *Local spin susceptibility*

In vanadium oxides, K is generally composed of the T-independent orbital (Van Vleck) term K_{VV} and the T-dependent spin one K_{spin}. As seen in Fig. 6, the experimental

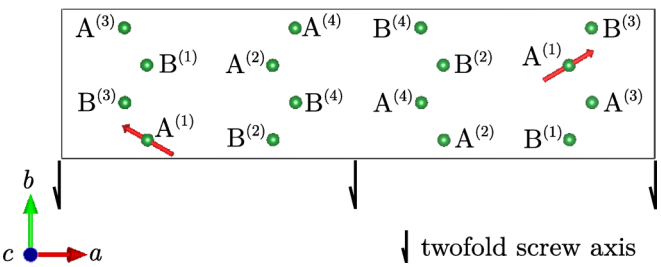

FIG. 5. The V3A$^{(1)}$–V3A$^{(4)}$ and V3B$^{(1)}$–V3B$^{(4)}$ sites viewed from the c axis in the $2a \times 2b \times c$ unit cell. The figure is based on the possible crystal structure with the space group of $P2_1$ discussed in Sec. IV B. Twofold screw axes are also presented in the figure. The red arrows represent one of the principal axes of the EFG tensor y_Q for the V3A$^{(1)}$ site.

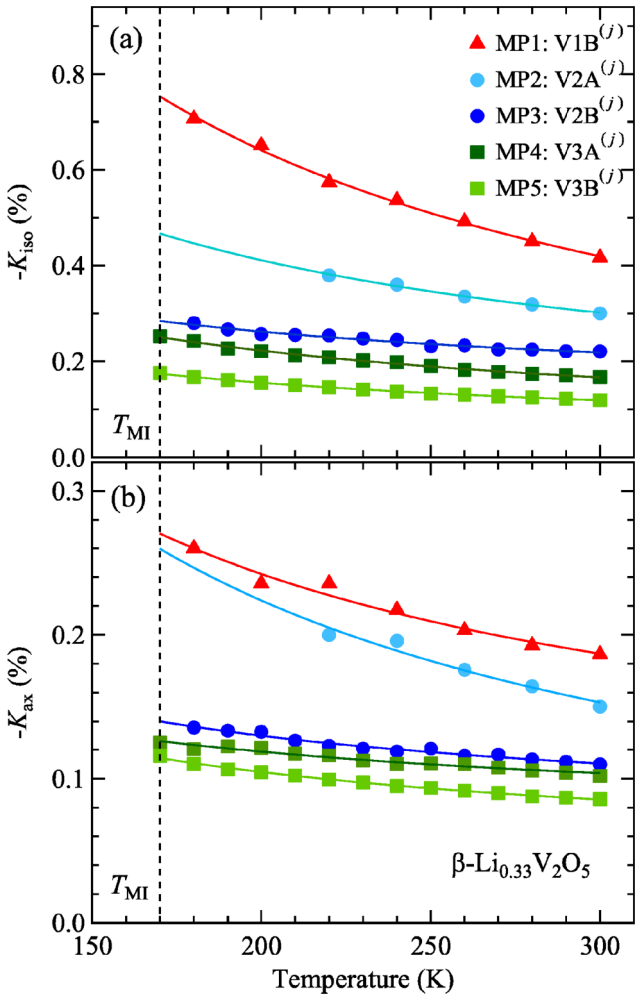

FIG. 6. Temperature dependence of (a) isotropic and (b) axially anisotropic ^{51}V Knight shifts for the ^{51}V NMR spectra MP1, MP2, MP3, MP4, and MP5 coming from the V1B$^{(j)}$, V2A$^{(j)}$, V2B$^{(j)}$, V3A$^{(j)}$, and V3B$^{(j)}$ ($j = 1$–n) sites, respectively, in β-Li$_{0.33}$V$_2$O$_5$. The solid curves represent the results of fitting the data to the Curie-Weiss law.

data of K can be well fitted to the Curie-Weiss (CW) law $K(T) = K_1/(T - \Theta) + K_0$ with the T-independent Knight shift K_0, a constant K_1, and the Weiss temperature Θ which is assumed as $\Theta = -18$ K of bulk magnetic susceptibility χ. Then, we found that $K_{VV}(=K_0)$ for MP3, MP4, and MP5 are negligibly small, whereas $(K^X_{VV}, K^Z_{VV}) = (0.17\%, 0.23\%)$ for MP1 and (0.00%, 0.16%) for MP2. The CW term in K, $K_{spin}(i)$ for $i =$ MP1, MP2, MP3, MP4, and MP5, is written by $K_{spin}(i) = A_{hf}\chi_{spin}(VX^{(j)})/N_A\mu_B$ where $X =$ 1B, 2A, 2B, 3A, and 3B, respectively, and $j = 1$–n. Here, N_A is the Avogadro's number, μ_B is the Bohr magneton, and A_{hf} is a hyperfine coupling constant [41]. To evaluate the isotropic local spin susceptibility $\chi_{spin}(VX^{(j)})$ from K_{iso}, we have to know the A_{hf} value due to the core-polarization mechanism for each vanadium site. However, the existence of several vanadium sites prevents us from estimating A_{hf} by the conventional K-χ analysis. Thus, we neglect the vanadium-site dependence of A_{hf} and assume a value of $A_{hf} = A_{iso} = -100$ kOe/μ_B, a standard value in 3d transition-metal compounds [42,43]. The obtained $\chi_{spin}(VX^{(j)})$ is presented in Fig. 7. Here, note that

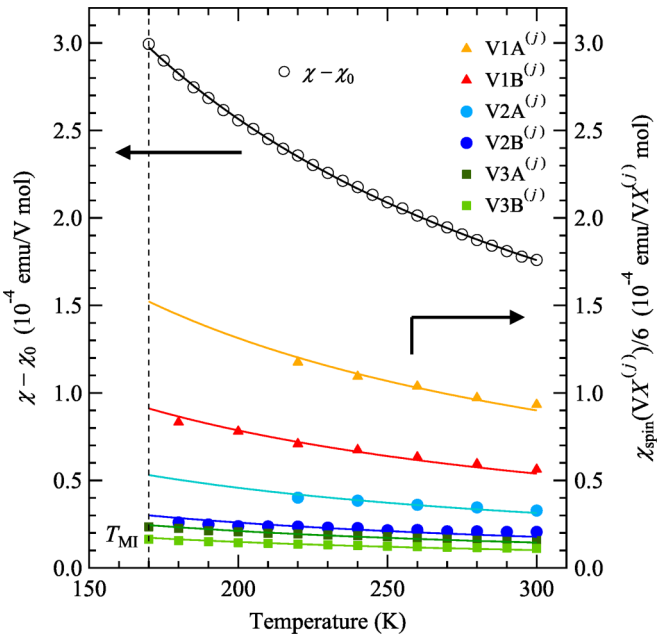

FIG. 7. Temperature dependence of isotropic spin susceptibility after subtracting a constant term χ_0 from magnetic susceptibility of a powder sample χ and local isotropic spin susceptibility $\chi_{spin}(VX^{(j)})$ ($X =$ 1A, 1B, 2A, 2B, 3A, and 3B; $j = 1$–n) in the metallic phase of β-Li$_{0.33}$V$_2$O$_5$. Note that $\chi_{spin}(VX^{(j)})$ is independent of j. The solid curves represent the results of fitting the data to the Curie-Weiss law.

$\chi_{spin}(VX^{(j)})$ is independent of j. The isotropic spin susceptibility χ_{spin}, which is calculated from subtracting a constant term χ_0 from magnetic susceptibility of the powder β-Li$_{0.33}$V$_2$O$_5$ sample χ, obeys the CW law $\chi_{spin}(=\chi - \chi_0) = C/(T - \Theta)$ where $C = 5.59 \times 10^{-2}$ K emu/V mol, $\Theta = -18$ K, and $\chi_0 = 5.2 \times 10^{-5}$ emu/V mol. Also, $\chi_{spin}(V1A^{(j)})$ is evaluated by subtracting $\sum_X \sum_j \chi_{spin}(VX^{(j)})$ for $X =$ 1B, 2A, 2B, 3A, and 3B from χ_{spin}. From the results of fitting the $\chi_{spin}(VX^{(j)})$ data to the CW law, the effective magnetic moment μ_{eff} is obtained as 1.17, 0.91, 0.69, 0.52, 0.47, and 0.39 in the units of μ_B for V1A$^{(j)}$, V1B$^{(j)}$, V2A$^{(j)}$, V2B$^{(j)}$, V3A$^{(j)}$, and V3B$^{(j)}$, respectively. A fact that χ_{spin} of V1A$^{(j)}$ is the largest among the V sites is consistent with the wipeout of the NMR signal coming from the V1A$^{(j)}$ sites due to a short T_2. The effective moment μ_{eff} is given as $\mu_{eff} = 2\mu_B\sqrt{s(s+1)}$ for orbital-quenched systems, where the spin s may be proportional to 3d electron number, n_e. Thus, we can roughly estimate n_e for each V site by taking account of the d electron distribution, one d electron per the six V sites, following the ratio of s. The n_e value is obtained as 0.27, 0.20, 0.17, 0.15, 0.11, and 0.09 for the V1A$^{(j)}$, V1B$^{(j)}$, V2A$^{(j)}$, V2B$^{(j)}$, V3A$^{(j)}$, and V3B$^{(j)}$ sites, respectively. For the $A =$ Na system, the electron distribution obtained from the ^{51}V NMR measurement similar to the present one was confirmed by the angular dependence of ^{23}Na Knight shift [32]. However, the poor precision in the ^{7}Li Knight shift prevented us from determining the electron distribution in β-Li$_{0.33}$V$_2$O$_5$.

3. *Spin dynamics*

Next, we turn our attention to the spin dynamics in β-Li$_{0.33}$V$_2$O$_5$. Figure 8 shows the T dependencies of the

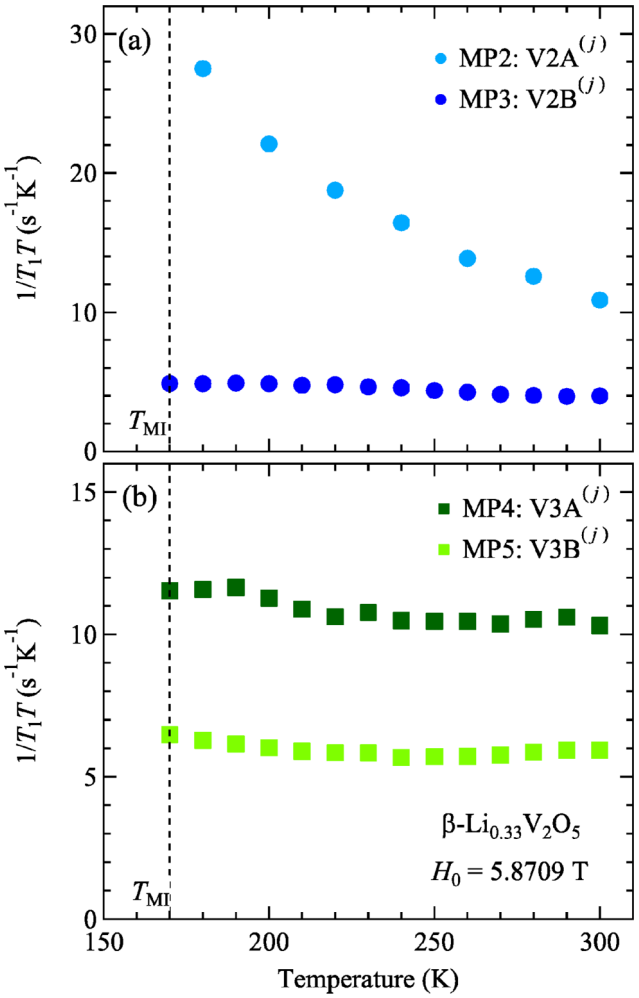

FIG. 8. Temperature dependence of $1/T_1T$ for the (a) MP2, MP3, (b) MP4, and MP5 spectra coming from the V2A$^{(j)}$, V2B$^{(j)}$, V3A$^{(j)}$, and V3B$^{(j)}$ (j = 1–n) sites, respectively, in the metallic phase of β-Li$_{0.33}$V$_2$O$_5$.

^{51}V nuclear spin-lattice relaxation rate divided by temperature $1/T_1T$ for the MP2, MP3, MP4, and MP5 spectra coming from the V2A$^{(j)}$, V2B$^{(j)}$, V3A$^{(j)}$, and V3B$^{(j)}$ (j = 1–n) sites, respectively. These data were measured for magic angles where the electric quadrupole splitting vanishes. Absence of the magic angle prevented us from measuring $1/T_1$ for MP1. As shown in Fig. 8(a), $1/T_1T$ for MP2 shows a steep increase with decreasing T, whereas the T dependence of $1/T_1T$ for MP3 is suppressed. Also, $1/T_1T$ of MP4 and MP5 are almost T independent.

$1/T_1T$ can monitor the spin dynamics via dynamical susceptibility [44]. As discussed in the Na [45,46] and Sr [35] systems, we analyzed the spin dynamics of the Li system based on the 1D electron gas model. For 1D conductors, the energy versus wave-number dispersion crosses the Fermi energy E_F only along one direction in k space. In such a situation, the low-energy electron-hole excitation is limited to the wave number $q \sim 0$ and $q \sim 2k_F$ (k_F: the Fermi wave number) modes as shown in the inset of Fig. 9 [47]. Thus, $1/T_1T$ is expressed as sum of $q \sim 0$ and $q \sim 2k_F$ contributions, $1/T_1T = (1/T_1T)_0 + (1/T_1T)_{2k_F}$ with

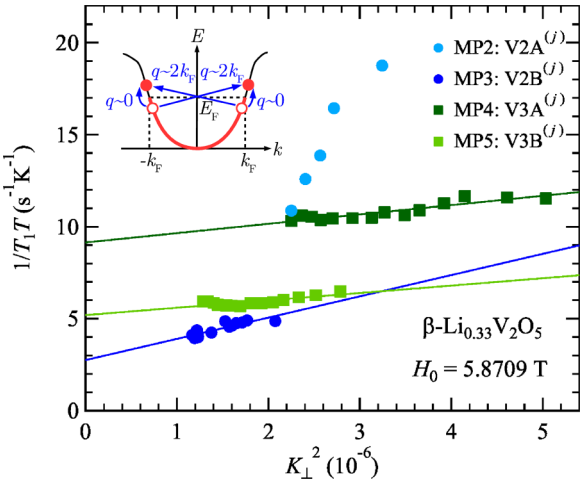

FIG. 9. $1/T_1T$ versus $K_\perp^2$ plots for the ^{51}V NMR spectra MP2, MP3, MP4, and MP5 coming from the V2A$^{(j)}$, V2B$^{(j)}$, V3A$^{(j)}$, and V3B$^{(j)}$ (j = 1–n) sites, respectively, in the metallic phase of β-Li$_{0.33}$V$_2$O$_5$. Solid lines are the results of fitting the data to the one-dimensional electron gas model as described in text. The inset schematically represents electron-hole excitations around the Fermi level E_F and the Fermi wave numbers $\pm k_F$ in the one-dimensional model.

$(1/T_1T)_0 = C_0K_\perp^2$ and $(1/T_1T)_{2k_F} = C_1T^{K_\rho-1}$ where C_0 and C_1 are the coupling constants, $K_\perp$ is the average value of the Knight shift perpendicular to the field direction, and K_ρ is the Tomonaga-Luttinger parameter [46–48]. Then, $K_\rho = 1$ corresponds to the noninteracting electrons, whereas $0 < K_\rho < 1$ for the repulsive interactions. In the noninteracting case, we can easily find the relation $1/T_1T = C_0K_\perp^2 + C_1$.

Figure 9 displays the $1/T_1T$ versus $K_\perp^2$ plot. As seen in Fig. 9, the MP3 data obey the 1D electron gas model in the weak interacting case, whereas the MP2 behavior not following the weak interacting case shows that the electron-electron interaction contributes to the spin dynamics of MP2. On the other hand, the spin dynamics of MP4 and MP5 are explained by the weak interacting case with the more dominant $q \sim 2k_F$ contribution than that of MP3 as seen in the tiny slope of the fitted results, namely, the small coupling constant for the $q \sim 0$ component C_0 in Fig. 9. Thus, we can conclude that the two V2 sites show much different behaviors from each other from the aspect of the spin dynamics. This contrasted behavior was also found in the A-cation ordered metallic phase of β-Na$_{0.33}$V$_2$O$_5$ [49] and β-Sr$_{0.33}$V$_2$O$_5$ [35]. The presence of the site-dependent electron correlation revealed by the present $1/T_1$ measurements may provide the difference in electron number among the VS (S = 1–3) sites as mentioned in Sec. III A 2.

B. Insulating phase

We now proceed to the ^{51}V NMR results in the insulating phase (IP) of β-Li$_{0.33}$V$_2$O$_5$. Below T_{MI}, many vanadium sites are expected to appear due to the charge order. We observed many sharp and broad peaks coming from many distinct V sites. Figure 10(a) shows the ^{51}V spectra measured for an interval between the first ($\pi/2$) and the second (π) pulses

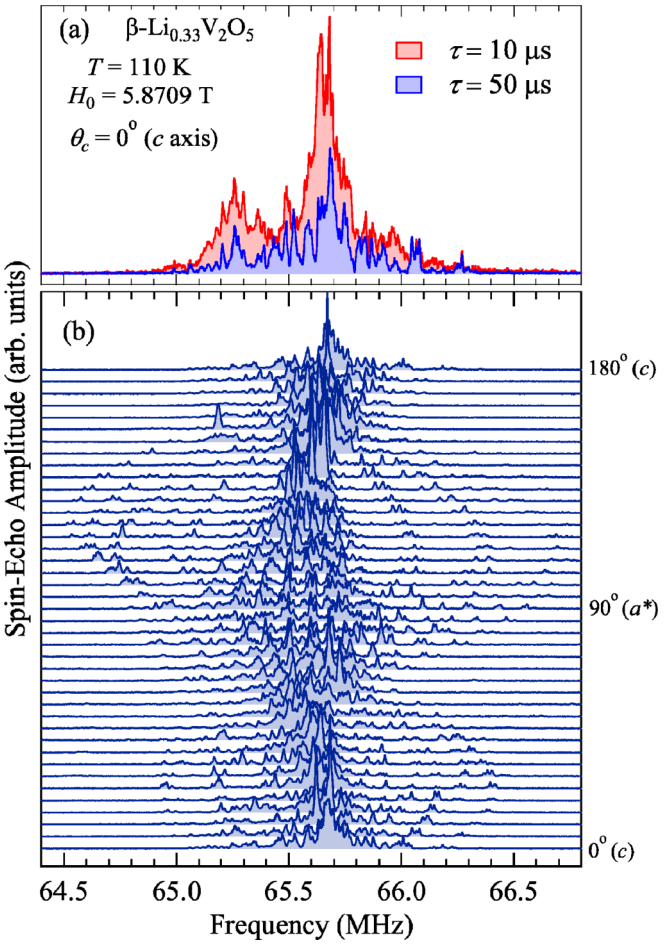

FIG. 10. (a) ^{51}V NMR spectra measured with an interval between two pulses $\tau = 7$ (red) and 50 (blue) μs and H_0 (=5.8709 T) parallel to the c axis at 110 K in β-$Li_{0.33}V_2O_5$. (b) Angular dependence of the ^{51}V NMR spectrum measured with $\tau = 50$ μs and H_0 rotated in the ca^* plane at 110 K.

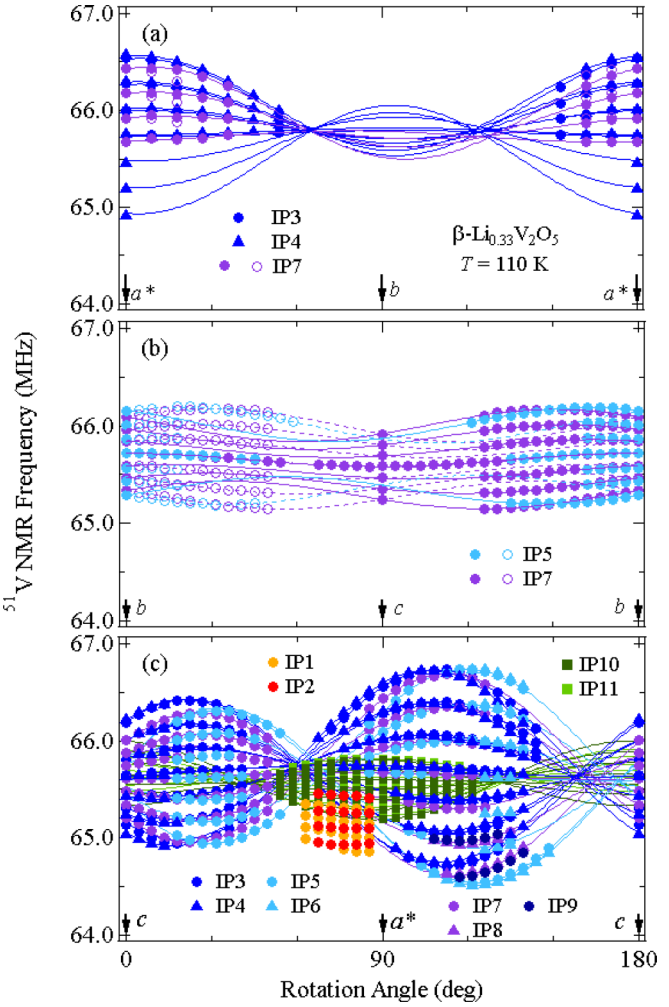

FIG. 11. Angular dependence of the ^{51}V NMR frequency of the IP1–IP11 spectra at 110 K with $H_0 = 5.8709$ T rotated in the (a) a^*b, (b) bc, and (c) ca^* planes of β-$Li_{0.33}V_2O_5$. Solid and dashed curves are the calculated results using the relation $\nu = \delta\nu_{m\leftrightarrow m-1}/2 + (1+K)\nu_0$ and the fitted EFG and K values listed in Table II.

$\tau = 7$ and 50 μs at 110 K with $H_0 \| c$. The ^{51}V spectrum for $\tau = 7$ μs is composed of many unresolvable broad components, whereas they relatively vanish due to short T_2 values in the spectrum for $\tau = 50$ μs. This means that they are ascribed to magnetic V sites whereas the spectrum for $\tau = 50$ μs mainly comes from nonmagnetic V^{5+} ($3d^0$) sites expected to appear in the insulating phase. Thus, Fig. 10(b) mainly shows the angular dependence of the nonmagnetic ^{51}V NMR spectrum at 110 K with H_0 rotated in the ca^* plane. As shown in our previous ^{23}Na NMR study [32], ^{7}Li NMR seems to be useful to determine the CO pattern. However, ^{7}Li NMR spectra became broad and unresolvable below T_{MI}. This broadening prevented us to obtain any information about the CO pattern.

From the complicated spectrum in Fig. 10(b), we could successfully pick up 11 sets of ^{51}V NMR spectra, IP1–IP11. Angular variations of the ^{51}V NMR frequencies and Knight shifts are summarized in Figs. 11 and 12, respectively. Without any sophisticated analysis, we are able to assign them into two V1, seven V2, and two V3 spectra from comparing Fig. 11 with Fig. 3. Here, note that the solid and open symbols in Figs. 11 and 12 come from one crystallographically equivalent V site with a local symmetry providing two types of principal axes in the K and EFG tensors as mentioned in Sec. III A 1. In Fig. 11, we denote the two V1 spectra as IP1 and IP2, the seven V2 ones as IP3–IP9, and the two V3 spectra as IP10 and IP11 for the observed eleven sets of ^{51}V NMR spectra. We analyzed these data by the same method as mentioned in Sec. III A 1 and could obtain the principal values and the direction of the principal axes of the K and EFG tensors for some sets in the 11 sets of spectra at 110 K as listed in Table II.

As seen in Table II, the observed V2 (V3) spectra have the K_{iso} values from -0.092% (-0.146%) to 0.014% (-0.108%) which are in magnitude smaller than the shifts in the metallic phase. Similar K values were also observed for the V^{5+} sites in the CO state of β-$Na_{0.33}V_2O_5$ [31]. Thus, the observed spectra are ascribed to the V^{5+} sites which have a transferred hyperfine (TH) interaction with the magnetic sites. In particular, the nonmagnetic V2 sites have the weakest TH interaction among the nonmagnetic V1–V3 sites. Also, it should be noted that the observed spectra can be divided into four groups, "IP3, IP4" (blue circles and triangles with blue curves, respectively), "IP5, IP6" (light blue ones), "IP7, IP8" (purple ones), and IP9

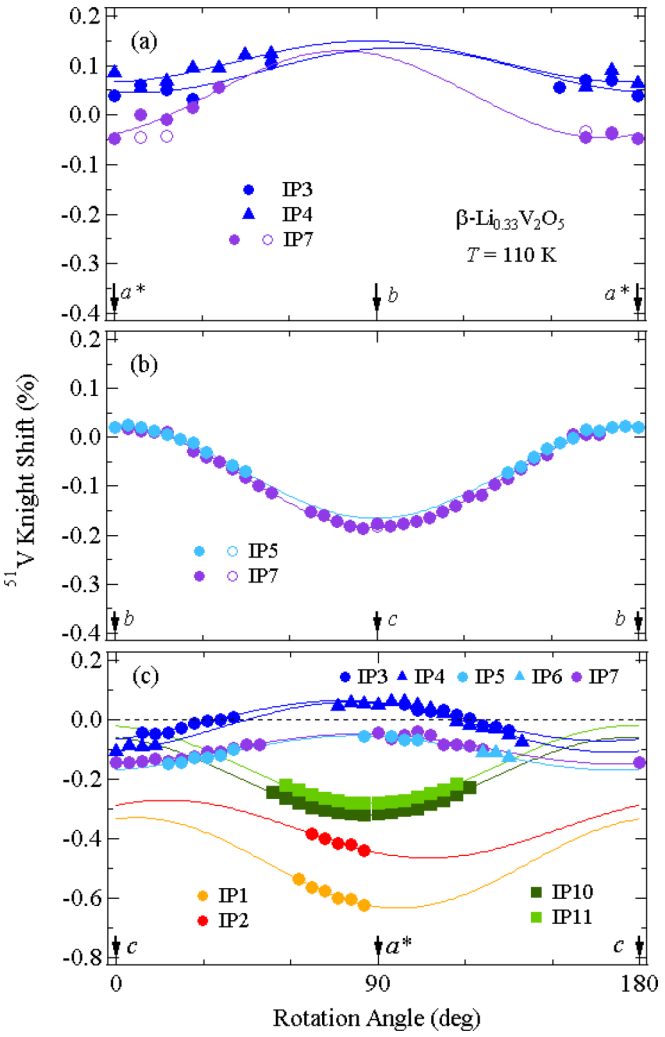

FIG. 12. Angular dependence of the ^{51}V Knight shift of the IP1–IP7, IP10, and IP11 spectra at 110 K in the (a) a^*b, (b) bc, and (c) ca^* planes of β-$Li_{0.33}V_2O_5$. Solid and dashed curves are the results of fitting the data to Eq. (2).

(dark blue circles), based on the angular dependence of the NMR frequency, as seen in Fig. 11(c). This means that the two spectra in each group come from the two V^{5+} sites with the local structure similar to each other.

IV. DISCUSSION

A. Electronic structure

Recently, the orbital-resolved NMR has been shown to be a useful technique for obtaining the electron occupation of each orbital in the 3d multiorbital systems [10,50,51]. Based on the information of the 3d orbital, we will discuss the electronic structure in β-$Li_{0.33}V_2O_5$. In the present t_{2g} system, $\chi_{\rm spin}(VX^{(j)})$ (X = 1A, 1B, 2A, 2B, 3A, and 3B, and j = 1–n) is described as the sum of magnetic susceptibility of each t_{2g} orbital, $\chi_{\rm spin}(VX^{(j)}) = \sum_k f_k \chi_{\rm spin}(VX^{(j)})$, where f_k ($k = xy$, yz, and zx) is a fraction of the d_k orbital and $\sum_k f_k = 1$. Based on the discussion in Refs. [10,50,51], $A_{\rm iso}$ and $A_{\rm ax}$ in t_{2g} systems are described as $A_{\rm iso} = -\kappa\langle r^{-3}\rangle$ and $A_{\rm ax} = -\frac{1}{7}\langle r^{-3}\rangle(2f_{xy} - f_{yz} - f_{zx})$, where $\langle r^{-3}\rangle$ is an expectation value of r^{-3} for the d orbital and κ is a dimensionless parameter of the Fermi contact interaction due to the core-polarization mechanism ($\kappa \sim 0.5$ for vanadates [52]). Thus, $K^{\rm ax}_{\rm spin}/K^{\rm iso}_{\rm spin}$ is written as $K^{\rm ax}_{\rm spin}/K^{\rm iso}_{\rm spin} = \frac{2}{7}(3f_{xy} - 1)$. From the experimental values of $K^{\rm ax}_{\rm spin}/K^{\rm iso}_{\rm spin}$ for the Li, Na [31], Ag [33,34], and Sr [35] systems, we obtain the f_{xy} values as listed in Table III where uncertain estimation of orbital susceptibilities in the Ag and Sr systems provides the approximate values of f_{xy}. These results show that the Knight shifts are largely anisotropic and the d electrons mainly occupy the d_{xy} orbital in β-$A_{0.33}V_2O_5$. Doublet and Lepetit calculated transfer integrals and magnetic exchange interactions, based on the d_{xy}-type orbital ordering expected from the distorted O^{2-} pyramidal coordination around the V sites in β-$Sr_{0.33}V_2O_5$, and proposed the structure of dominant interactions composed of the weakly coupled three two-leg ladders: two V1-V3 and one V2-V2 ladders [53]. This model is also applicable to the electronic structure of β-$Li_{0.33}V_2O_5$ as seen in Table III where the average values of f_{xy} for the $VSA^{(j)}$ and $VSB^{(j)}$ (S = 1–3) sites are presented in β-$Li_{0.33}V_2O_5$.

The low fraction of the d_{xy} orbital at the V1 site, as seen in Table III, shows that the d electrons at the V1 site are shared

TABLE II. Principal components of the ^{51}V Knight shift, K_x and K_z, the electric quadrupole frequency $\nu_{\rm Q}$, the asymmetry parameter of EFG η, and directions of principal axes of the K and EFG tensors $z_{\rm K}$ and $z_{\rm Q}$ projected on the ca^* plane for the IP1–IP11 spectra coming from the V^{5+} sites at 110 K in β-$Li_{0.33}V_2O_5$. The V sites which may lead to the observed NMR spectra are also presented in a proposed CO model as shown in Fig. 14(d).

Spectrum	V site	K_x (%)	K_z (%)	$z_{\rm K}$ [θ_b (°)]	$\nu_{\rm Q}$ (MHz)	η	$z_{\rm Q}$ [θ_b (°)]
IP1	$V1A^{(1)}$						
IP2	$V1D^{(1)}$						
IP3	$V2A^{(1)}$	0.064	−0.071	168	0.338	0.449	110
IP4	$V2D^{(1)}$	0.078	−0.113	172	0.334	0.476	108
IP5	$V2A^{(2)}$	−0.054	−0.170	173	0.366	0.242	121
IP6	$V2D^{(2)}$						
IP7	$V2A^{(3)}$	−0.041	−0.151	174	0.346	0.265	114
IP8	$V2D^{(3)}$						
IP9	$V2A^{(4)}$						
IP10	$V3A^{(1)}$	−0.060	−0.319	86	0.111	0.838	177
IP11	$V3D^{(1)}$	−0.021	−0.281	87	0.100	0.420	87

TABLE III. Fraction of the d_{xy} orbital contribution to spin susceptibility, f_{xy}, of each V site estimated from the ^{51}V Knight shifts in the A-ordered metallic state of β-$A_{0.33}V_2O_5$ (A = Li, Na [31], Ag [33,34], and Sr [35]).

	V1	V2	V3
β-$Li_{0.33}V_2O_5$	0.7	0.9	1.0
β-$Na_{0.33}V_2O_5$		0.9	1.0
β-$Ag_{0.33}V_2O_5$	~0.7	~1.0	~1.0
β-$Sr_{0.33}V_2O_5$	~0.8	~0.9	~1.0

by the d_{xy} and d_{yz}/d_{zx} orbitals. Thus, the V1 site has an energy gain due to the interorbital Coulomb interaction in comparison with the V2 and V3 sites governed by only the intraorbital one. This naturally explains the largest electron density observed for the V1 site.

B. Charge disproportionation in metallic phase

First, we discuss the crystal structure of β-$Li_{0.33}V_2O_5$ from the present NMR results to determine the CD pattern. Since the observed NMR spectra in the metallic phase of β-$Li_{0.33}V_2O_5$ are similar to those of other β-$A_{0.33}V_2O_5$, we take the monoclinic $P2_1/a$ structure with the $a\times2b\times c$ unit cell, which has been observed in the A-ordered metallic phase of other β-$A_{0.33}V_2O_5$, as a starting point. In the $P2_1/a$ structure, there are three types of symmetry operation: the inversion center, a-glide plane, and twofold screw axis [32]. If the $2a$ superlattice modulation appears in the structure due to the Li ordering, the inversion center and a-glide plane are vanished, whereas the twofold screw axis can be conserved as shown in Fig. 5. Indeed, if there is the twofold screw axis parallel to the b axis, we can explain that two sets of observed NMR spectra, which are shown by the solid and dashed lines in Fig. 2, and solid and open symbols in Figs. 3 and 4, come from one crystallographically equivalent site. Since there is no space group only having the twofold screw axis except $P2_1$, the crystal structure in the metallic phase of β-$Li_{0.33}V_2O_5$ likely has the space group $P2_1$. In this crystal structure, each VX (X = 1A, 1B, 2A, 2B, 3A, and 3B) site splits into four crystallographically inequivalent sites V$X^{(1)}$–V$X^{(4)}$. Detailed x-ray and neutron diffraction studies are required to confirm this crystal structure.

In the metallic phase of β-$Na_{0.33}V_2O_5$ and β-$Ag_{0.33}V_2O_5$, the CD takes place as shown in Figs. 13(a) and 13(b), respectively, where the CD pattern is presented on the weakly coupled ladder as a structural unit [32–34]. The $3d$ electron number of V1, V2, and V3 is roughly estimated as 0.25, 0.14, and 0.11, respectively, in β-$Na_{0.33}V_2O_5$ [32], whereas each site has almost the same $3d$ electron number in β-$Ag_{0.33}V_2O_5$ [33,34]. Figures 13(c) and 13(d) show a possible model of the CD pattern in the metallic phase of β-$Li_{0.33}V_2O_5$ based on the $P2_1$ crystal structure with the $2a\times2b\times c$ modulation. Within this model, the observed MP1–MP5 spectra come from the V1B$^{(1)}$–V1B$^{(4)}$, V2A$^{(1)}$–V2A$^{(4)}$, V2B$^{(1)}$–V2B$^{(4)}$, V3A$^{(1)}$–V3A$^{(4)}$, and V3B$^{(1)}$–V3B$^{(4)}$ sites, respectively, as presented in Table I. The CD pattern also has the $3d$ electron number of the V1A$^{(j)}$, V1B$^{(j)}$, V2A$^{(j)}$, V2B$^{(j)}$, V3A$^{(j)}$, and V3B$^{(j)}$ sites which is roughly estimated as 0.27, 0.20, 0.17, 0.15, 0.11, and 0.09, respectively, on the weakly coupled ladder as mentioned in Sec. III A 2.

From the present NMR results, we can deduce two important aspects of the electronic state in the metallic phase of β-$Li_{0.33}V_2O_5$. First, although all the V sites contribute to the electronic structure as the coupled-ladders model, each VS (S = 1–3) site has the electron number different from each other and it is the largest at the V1 site similar to β-$Na_{0.33}V_2O_5$. This result indicates that the coupled-ladders model contains two types of V ladders having different electron filling. Second, the zigzag ordering of the A ion leads to the CD as discussed in δ-$Ag_{2/3}V_2O_5$ [54]. One possible process which induces the CD may take place via a distribution of the Coulomb potential at the V sites. In β-$A_{0.33}V_2O_5$, the V2A or V2B site on a V2-V2 ladder has one neighboring A ion, whereas the V1A, V1B, V3A, or V3B site on a V1-V3 ladder has two ones. This local structure leads to the large difference between the Na-V2A distance of 3.83 Å and the Na-V2B one of 4.98 Å compared with the difference between Na-V1A (Na-V3A) of 3.71 (3.63) Å and Na-V1B of 3.70 (3.65) Å (Na-V3B) in β-$Na_{0.33}V_2O_5$ [27]. Thus, the $3d$ electron number at the V2A site is expected to be higher than that of V2B via the Coulomb potential generated by the Li^+ ions. On the other hand, there is not a local structural feature which is able to induce the CD between the V1A and V1B (V3A and V3B) sites. The difference between the $3d$ electron numbers of the V1A and V1B (V3A and V3B) sites may be induced by the CD in the V2-V2 ladders because these V sites share the d electrons via the interchain interactions which are ascribed to the mixing of the d_{xy} orbitals via the corner sharing between $V1O_6$ ($V3O_5$) and $V2O_6$ [31]. Therefore, the difference in electron number is expected to be the largest between the V2A and V2B sites. However, the largest one is between V1A and V1B sites, as the ratio of the electron numbers for VSA and VSB (S = 1–3) sites, n_e(VSA)/n_e(VSB), is 1.35, 1.13, and 1.22 for S = 1, 2, and 3, respectively. Thus, although the CD pattern may be driven by the Li zigzag ordering, the electron number of each V site seems to be governed by t_l ($l = \parallel$, $\perp$, and inter) which are the electron hopping energies (along the leg, rung, and interladder directions, respectively), the onsite Coulomb energy U and the intersite Coulomb energy V as discussed below. These parameters are also considered to govern the spin dynamics mentioned in Sec. III A 3.

Although the characteristic feature of the CD mentioned above is commonly seen in β-$A_{0.33}V_2O_5$ [35,36], we can particularly find quantitative difference in charge density at the V sites depending on the A cation. Among the Li, Na, and Ag systems, the Li system has the largest difference in the local magnetic properties of the V sites [31,36,49], whereas the Ag system shows little difference [33,34]. These findings may be ascribed to the difference in t_l/U. In particular, $t_\parallel/U$ generally becomes small to stabilize the insulating CO phase. Therefore, if $t_\parallel/U$ in the Li system is the smallest among the Li, Na, and Ag systems, we may explain that the Li system has the highest T_{MI} (=170 K for Li, 135 K for Na, and 90 K for Ag) and the highest critical pressure, above which the MI transition disappears, P_c [15,20,23–25]. This should be confirmed by determining the t_l, U, and V values based on the first-principles calculation for β-$A_{0.33}V_2O_5$ (A = Li, Na, and Ag). A theoretical simulation based on these parameters is

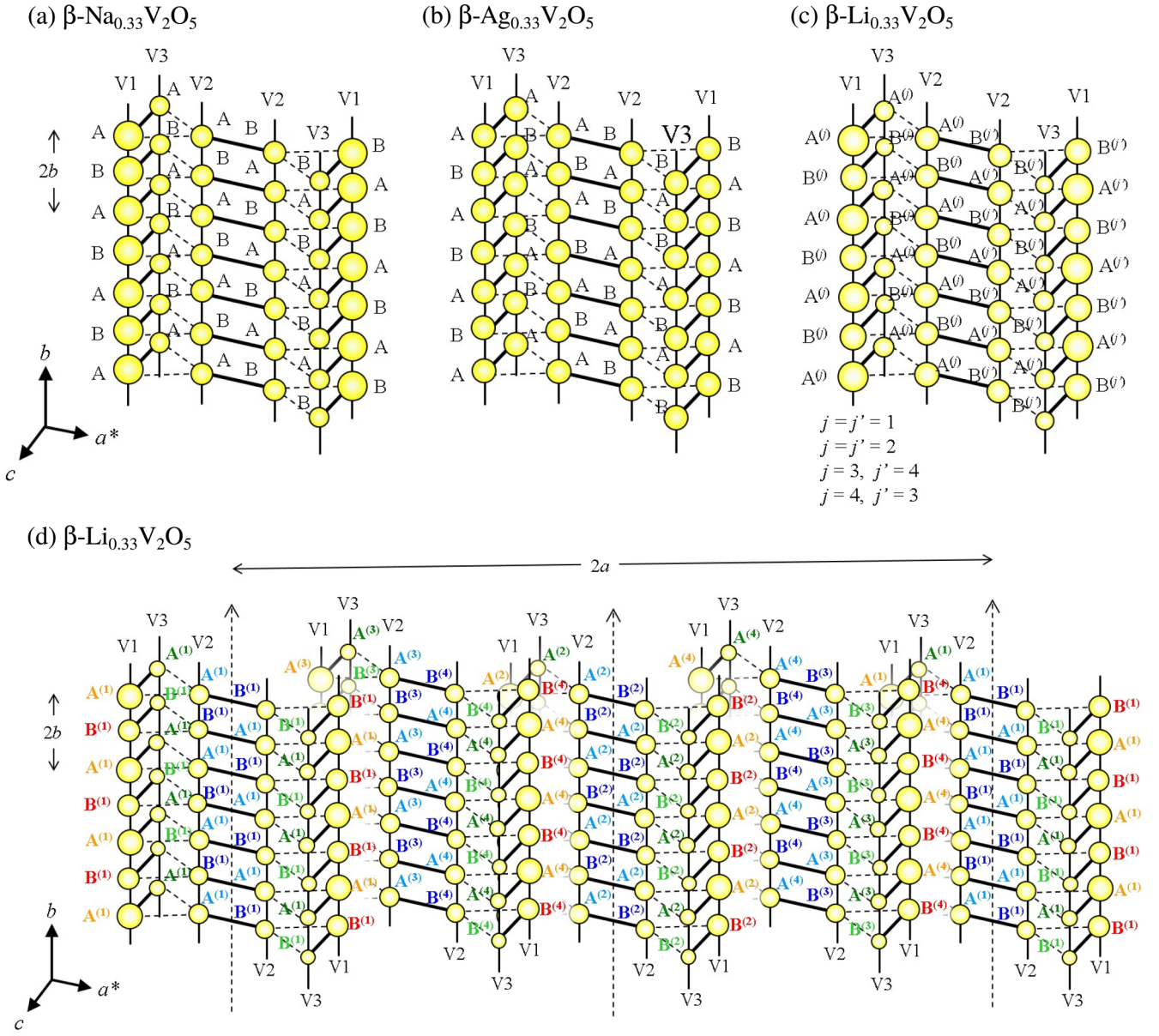

FIG. 13. Schematic figure of the charge disproportionation on the weakly coupled ladders model in the metallic phase of (a) β-$Na_{0.33}V_2O_5$ [32], (b) β-$Ag_{0.33}V_2O_5$ [33,34], and (c) β-$Li_{0.33}V_2O_5$. (d) A possible modulation along the a axis for the Li system. The area of the circle at each V site is proportional to the electron number. The dotted arrows represent the twofold screw axes. The color of the symbols for the V sites in (d) corresponds to the color of the NMR spectra in the metallic phase.

also desired to reproduce the site-dependent electron density in the CD pattern of β-$A_{0.33}V_2O_5$.

C. Charge order in insulating phase

The CO leading to the MI transition appears in the insulating phase of β-$A_{0.33}V_2O_5$. Up to now, the CO pattern in the Na system has been most intensively investigated among β-$A_{0.33}V_2O_5$. From NMR [31,32] and neutron scattering [19] measurements, the CO model with the V*S*A–V*S*F (S = 1–3) sites was proposed as presented in Fig. 14(a). The V*S*A and V*S*D sites are nonmagnetic, whereas the V*S*B, V*S*C, V*S*E, and V*S*F sites are magnetic. All of the six V^{5+} sites are aligned in the same ca plane in the coupled-ladders system and the wall of V^{5+} appears every three V sites along the b axis. This is also supported by a recent x-ray scattering measurement [55]. On the other hand, in β-$Ag_{0.33}V_2O_5$, a model was proposed to have the wall of the d-electron rich V sites which appears every three V sites along the b axis as shown in Fig. 14(b) [33,34].

We discuss the CO pattern in β-$Li_{0.33}V_2O_5$, based on the present ^{51}V NMR results in Sec. III B. The electron density, one d electron per six V ions, which governs the 6b modulation of the CO pattern in β-$A_{0.33}V_2O_5$ (A = Na and Ag), reasonably seems to result in the same modulation in β-$Li_{0.33}V_2O_5$. Furthermore, since we observed the splitting in the angular dependence of the NMR spectrum which can be explained by the existence of the twofold screw axis as shown in the solid

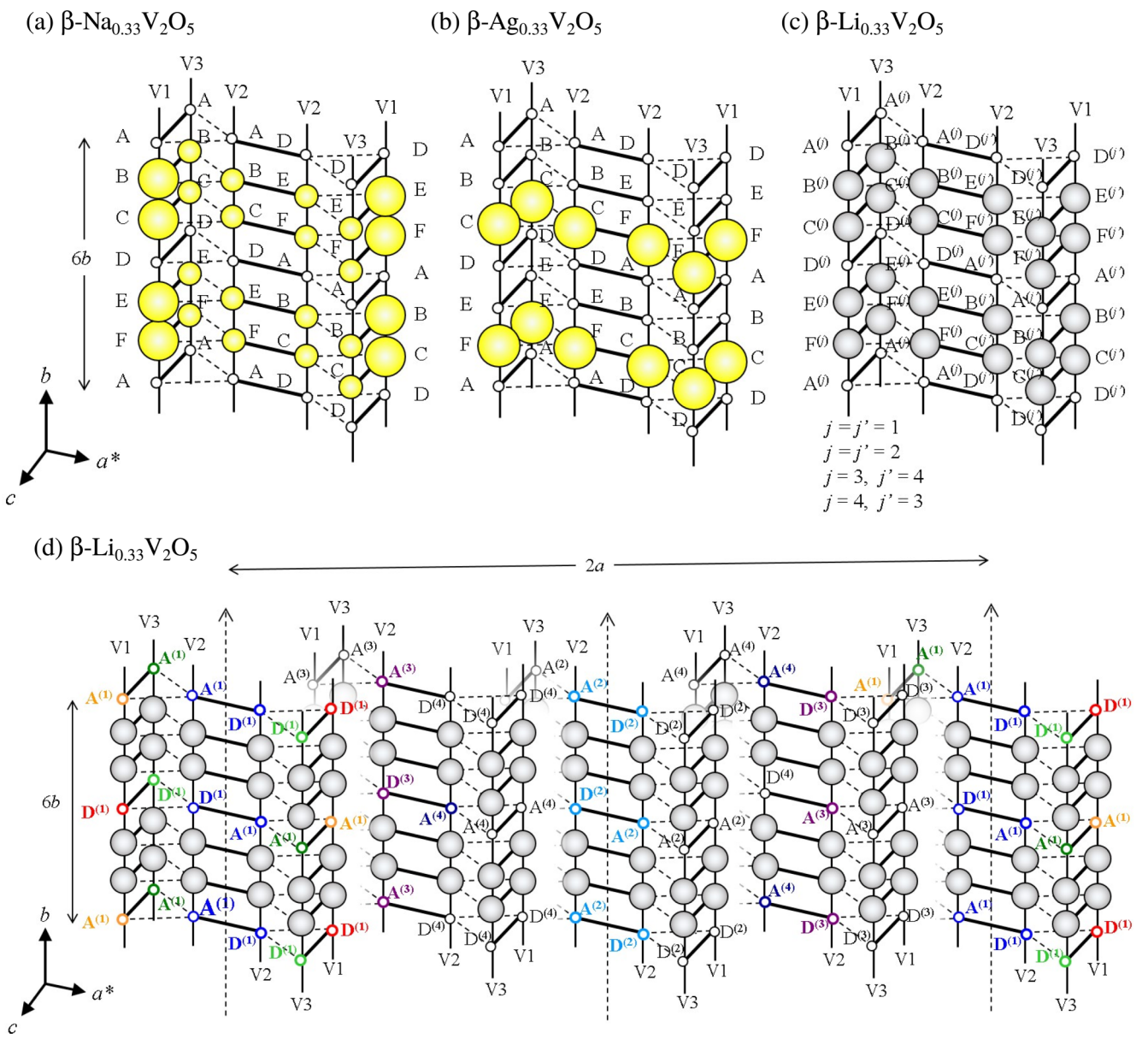

FIG. 14. Schematic charge-order pattern on weakly coupled three ladders in the insulating phase of (a) β-$Na_{0.33}V_2O_5$ [31], (b) β-$Ag_{0.33}V_2O_5$ [34], and (c) β-$Li_{0.33}V_2O_5$. (d) A possible modulation along the a axis for the Li system. The white circles represent the $V^{5+}(3d^0)$ sites, whereas the gray and yellow circles denote the $V^{(5-n_e)+}(3d^{n_e})$ sites where n_e is the $3d$-electron number. The n_e value is unknown for the gray circles, and the area of the yellow circles corresponds to n_e at the V sites. The dotted arrows represent the twofold screw axes. The color of the symbols for the V^{5+} sites in (d) corresponds to the color of the NMR spectra (Fig. 11) in the insulating phase except the black whose NMR spectrum is not observed.

and open symbols in Figs. 11(a) and 11(b), the $P2_1$ structure is still conserved in the CO state even with the $6b$ superlattice modulation, whereas the monoclinic $P2_1/a$ structure has been established in the CO state of the Na system. As discussed on the metallic phase, each of the original VY (Y = 1A–1F, 2A–2F, and 3A–3F) site is split into four crystallographically inequivalent sites, V$Y^{(1)}$–V$Y^{(4)}$, due to the lowering in the symmetry of the crystal structure from $P2_1/a$ to $P2_1$. As shown in Sec. III B, we observed seven sets of V^{5+} spectra from the V2 sites, IP3–IP9. This result is reasonably explained by the CO model similar to that of the Na system on the $P2_1$ structure with the $2a\times6b\times c$ unit cell. One possible CO pattern in β-$Li_{0.33}V_2O_5$ is depicted in Figs. 14(c) and 14(d). In this CO model, the V$SA^{(1)}$–V$SA^{(4)}$ and V$SD^{(1)}$–V$SD^{(4)}$ sites are nonmagnetic and the wall of the V^{5+} sites appears with the $3b$ modulation as observed in β-$Na_{0.33}V_2O_5$. The $6b$ modulation takes place due to the $3b$ electronic modulation in addition to the $2b$ Li modulation. The eight nonmagnetic V2 sites, V2$A^{(1)}$–V2$A^{(4)}$ and V2$D^{(1)}$–V2$D^{(4)}$, can provide the observed seven sets of V2 spectra. Although a similar splitting is expected for the V1 (V3) sites, we could only find the two sets of spectra IP1 and IP2 (IP10 and IP11). We consider that the two sets are originating from the two sites among the eight nonmagnetic V1 (V3) sites, V1$A^{(1)}$–V1$A^{(4)}$ and V1$D^{(1)}$–V1$D^{(4)}$ [V3$A^{(1)}$–V3$A^{(4)}$ and V3$D^{(1)}$–V3$D^{(4)}$], and the other V^{5+} spectra are hidden in the complicated spectra.

Other models may be able to reproduce the present NMR spectra. However, a lack of information on the detailed crystal structure and the insufficient observation of the ^{51}V NMR spectrum prevent us from determining the precise CO pattern.

Thus, the CO pattern in β-$A_{0.33}V_2O_5$ (A = Li, Na, and Ag) depends on the A cation, although the basic electronic structure is commonly described by the model of the weakly coupled two-leg ladders. The CO mechanism has been discussed from two approaches: the band nesting and the molecular orbital models. The CO in the Li and Na systems may be mainly ascribed to the band nesting due to the quasi-1D structure coming from the strong $t_{\parallel}$, whereas the strong $t_{\perp}$ may result in that the two V sites on the rung share one $3d$ electron every three V sites along the b axis in the Ag system [33,34]. From theoretical aspects, several studies partially reproduce the CO pattern in β-$A_{0.33}V_2O_5$. Tsuchiizu proposed a $4k_F$ CDW model on coupled three $\frac{1}{6}$-filled chains as an origin of CD and CO [56]. On the other hand, Seo *et al.* obtained a Hartree-Fock solution of the Hubbard model with the intraladder and interladder hopping and the onsite Coulomb interaction, where the transfer integrals are determined from the first-principles calculation [57]. However, based on these theoretical studies, the CO patterns in β-$A_{0.33}V_2O_5$ have not systematically been discussed. Also, the A-cation effect and the intersite Coulomb interaction should be taken into account in addition to the intraladder and interladder electron hopping and the onsite Coulomb interaction as discussed in several organic conductors [58] and α'-NaV_2O_5 [59]. Thus, theoretical studies based on realistic values of the interactions are desired to understand the A dependence of the CO and CD patterns of β-$A_{0.33}V_2O_5$ that we discussed in this study.

V. CONCLUSION

We reported ^{51}V NMR results on a single crystal of β-$Li_{0.33}V_2O_5$ which undergoes a metal-insulator transition at $T_{MI} \sim 170$ K accompanied by a charge ordering. Based on the ^{51}V Knight shifts and the nuclear spin-lattice relaxation rates above T_{MI}, we inferred a weakly coupled ladders model containing two types of ladders with distinct carrier densities as an electronic structure. We also proposed a charge disproportionation model with the superlattice structure $2a \times 2b \times c$ and inferred that the Li zigzag ordering induces the charge disproportionation with the charge density and the spin dynamics governed by electron hopping energies, onsite Coulomb energies, and intersite Coulomb energies. Below T_{MI}, we proposed a charge-ordering pattern with the superlattice structure $2a \times 6b \times c$ larger than that in other family members of β-vanadium bronze. We also suggested that the intraladder hopping in β-$Li_{0.33}V_2O_5$ is the smallest, which may lead to the highest T_{MI} and the highest critical pressure above which the superconducting phase appears, among β-$A_{0.33}V_2O_5$ (A = Li, Na, and Ag).

ACKNOWLEDGMENTS

We would like to thank M. Isobe, M. Tsuchiizu, H. Seo, A. Hisada, N. Fujiwara, T. Waki, M. Takigawa, H. Takeda, and Y. Shimizu for fruitful discussion, and S. Inoue for technical assistance. This study was supported by KAKENHI (Grants No. 19340097 and No. 16H04012) from the Japan Society for the Promotion of Science (JSPS). One of the authors (I.Y.) also thanks the JSPS for the financial support through the Grant-in-Aid for JSPS Fellows.

[1] M. Imada, A. Fujimori, and Y. Tokura, Rev. Mod. Phys. **70**, 1039 (1998).
[2] K. Hasegawa, M. Isobe, T. Yamauchi, H. Ueda, J.-I. Yamaura, H. Gotou, T. Yagi, H. Sato, and Y. Ueda, Phys. Rev. Lett. **103**, 146403 (2009).
[3] A. Nakao, Y. Yamaki, H. Nakao, Y. Murakami, K. Hasegawa, M. Isobe, and Y. Ueda, J. Phys. Soc. Jpn. **81**, 054710 (2012).
[4] M. Isobe, S. Koishi, S. Yamazaki, J. Yamaura, H. Gotou, T. Yagi, and Y. Ueda, J. Phys. Soc. Jpn. **78**, 114713 (2009).
[5] Y. Shimizu, K. Okai, M. Itoh, M. Isobe, J.-I. Yamaura, T. Yamauchi, and Y. Ueda, Phys. Rev. B **83**, 155111 (2011).
[6] A. C. Komarek, M. Isobe, J. Hemberger, D. Meier, T. Lorenz, D. Trots, A. Cervellino, M. T. Fernández-Diaz, Y. Ueda, and M. Braden, Phys. Rev. Lett. **107**, 027201 (2011).
[7] K. Yamaura, M. Arai, A. Sato, A. B. Karki, D. P. Young, R. Movshovich, S. Okamoto, D. Mandrus, and E. Takayama-Muromachi, Phys. Rev. Lett. **99**, 196601 (2007).
[8] H. Sakurai, Phys. Rev. B **78**, 094410 (2008).
[9] T. Qian, K. Nakayama, Y. Sun, T. Arakane, T. Sato, T. Takahashi, K. Yamaura, and E. Takayama-Muromachi, J. Phys. Soc. Jpn. **78**, 024709 (2009).
[10] H. Takeda, M. Itoh, and H. Sakurai, Phys. Rev. B **86**, 174405 (2012).
[11] H. Sakurai, T. Kolodiazhnyi, Y. Michiue, E. Takayama-Muromachi, Y. Tanabe, and H. Kikuchi, Angew. Chem. Int. Ed. **51**, 6653 (2012).
[12] H. Takeda, Y. Shimizu, M. Itoh, H. Sakurai, and E. Takayama-Muromachi, J. Korean Phys. Soc. **62**, 1914 (2013).
[13] H. Yamada and Y. Ueda, J. Phys. Soc. Jpn. **68**, 2735 (1999).
[14] Y. Ueda, H. Yamada, M. Isobe, and T. Yamauchi, J. Alloys Compd. **317-318**, 109 (2001).
[15] T. Yamauchi, M. Isobe, and Y. Ueda, Solid State Sci. **7**, 874 (2005).
[16] M. Itoh, N. Akimoto, H. Yamada, M. Isobe, and Y. Ueda, J. Phys. Soc. Jpn. Suppl. B **69**, 155 (2000).
[17] M. Itoh, N. Akimoto, H. Yamada, M. Isobe, and Y. Ueda, J. Phys. Chem. Solids **62**, 351 (2001).
[18] A. N. Vasil'ev, V. I. Marchenko, A. I. Smirnov, S. S. Sosin, H. Yamada, and Y. Ueda, Phys. Rev. B **64**, 174403 (2001).
[19] S. Nagai, M. Nishi, K. Kakurai, Y. Oohara, H. Yoshizawa, H. Kimura, Y. Noda, B. Grenier, T. Yamauchi, J. Yamaura, M. Isobe, Y. Ueda, and K. Hirota, J. Phys. Soc. Jpn. **74**, 1297 (2005).
[20] T. Yamauchi, Y. Ueda, and N. Môri, Phys. Rev. Lett. **89**, 057002 (2002).
[21] Y. Ueda, M. Isobe, and T. Yamauchi, J. Phys. Chem. Solids **63**, 951 (2002).

[22] G. Obermeier, D. Ciesla, S. Klimm, and S. Horn, Phys. Rev. B **66**, 085117 (2002).
[23] T. Yamauchi, H. Ueda, and Y. Ueda, Phys. C (Amsterdam) **460-462**, 66 (2007).
[24] T. Yamauchi and Y. Ueda, Phys. Rev. B **77**, 104529 (2008).
[25] T. Suzuki, I. Yamauchi, Y. Shimizu, M. Itoh, N. Takeshita, C. Terakura, H. Takagi, Y. Tokura, T. Yamauchi, and Y. Ueda, Phys. Rev. B **79**, 081101(R) (2009).
[26] A. D. Wadsley, Acta Crystallogr. **8**, 695 (1955).
[27] J.-I. Yamaura, M. Isobe, H. Yamada, T. Yamauchi, and Y. Ueda, J. Phys. Chem. Solids **63**, 957 (2002).
[28] J. Yamaura, T. Yamauchi, E. Ninomiya, H. Sawa, M. Isobe, H. Yamada, and Y. Ueda, J. Magn. Magn. Mater. **272-276**, 438 (2004).
[29] C. Sellier, F. Boucher, and E. Janod, Solid State Sci. **5**, 591 (2003).
[30] M. Heinrich, H.-A. Krug von Nidda, R. M. Eremina, A. Loidl, Ch. Helbig, G. Obermeier, and S. Horn, Phys. Rev. Lett. **93**, 116402 (2004).
[31] T. Suzuki, I. Yamauchi, M. Itoh, T. Yamauchi, and Y. Ueda, Phys. Rev. B **73**, 224421 (2006).
[32] M. Itoh, I. Yamauchi, T. Kozuka, T. Suzuki, T. Yamauchi, J.-I. Yamaura, and Y. Ueda, Phys. Rev. B **74**, 054434 (2006).
[33] A. Hisada, N. Fujiwara, T. Yamauchi, Y. Ueda, M. Hedo, and Y. Uwatoko, Phys. Rev. B **78**, 012402 (2008).
[34] A. Hisada, N. Fujiwara, T. Yamauchi, and Y. Ueda, J. Phys. Soc. Jpn. **78**, 094705 (2009).
[35] T. Waki, M. Takigawa, T. Yamauchi, J. Yamaura, H. Ueda, and Y. Ueda, J. Phys. Chem. Solids **68**, 2143 (2007).
[36] We observed that the V2 spectrum splits into two spectra coming from the V2A and V2B sites with different electron numbers in the Na ordered state of β-$Na_{0.33}V_2O_5$ after a previous ^{51}V NMR study, in which no splitting was reported, was published [31]. This result will appear elsewhere.
[37] I. Yamauchi, M. Itoh, T. Yamauchi, J.-I. Yamaura, and Y. Ueda, J. Phys.: Conf. Ser. **200**, 012234 (2010).
[38] I. Yamauchi, M. Itoh, T. Yamauchi, J.-I. Yamaura, and Y. Ueda, J. Phys.: Conf. Ser. **150**, 042236 (2009).
[39] J. Yamaura, T. Yamauchi, and Y. Ueda (unpublished).
[40] G. M. Volkoff, H. E. Petch, and D. W. Smellie, Can. J. Phys. **30**, 270 (1952).
[41] A. Abragam, *Principles of Nuclear Magnetism* (Oxford University Press, Oxford, 1961).
[42] A. Abragam and B. Bleaney, *Electron Paramagnetic Resonance of Transition Ions* (Clarendon, Oxford, 1970).
[43] T. Kiyama, H. Saitoh, M. Itoh, K. Kodama, H. Ichikawa, and J. Akimitsu, J. Phys. Soc. Jpn. **74**, 1123 (2005).
[44] T. Moriya, J. Phys. Soc. Jpn. **18**, 516 (1963).
[45] I. Yamauchi, M. Itoh, T. Yamauchi, and Y. Ueda, Phys. Rev. B **74**, 104410 (2006).
[46] I. Yamauchi, M. Itoh, T. Yamauchi, and Y. Ueda, J. Phys. Soc. Jpn. **77**, 104715 (2008).
[47] T. Giamarchi, Chem. Rev. **104**, 5037 (2004).
[48] C. Bourbonnais, J. Phys. I France **3**, 143 (1993).
[49] I. Yamauchi, T. Suzuki, Y. Shimizu, M. Itoh, T. Yamauchi, and Y. Ueda (unpublished).
[50] Y. Shimizu, S. Aoyama, T. Jinno, M. Itoh, and Y. Ueda, Phys. Rev. Lett. **114**, 166403 (2015).
[51] Y. Shimizu, H. Takeda, M. Tanaka, M. Itoh, S. Niitaka, and H. Takagi, Nat. Commun. **3**, 981 (2012).
[52] T. Kiyama, T. Shiraoka, M. Itoh, L. Kano, H. Ichikawa, and J. Akimitsu, Phys. Rev. B **73**, 184422 (2006).
[53] M.-L. Doublet and M.-B. Lepetit, Phys. Rev. B **71**, 075119 (2005).
[54] T. Baba, T. Yamauchi, S. Yamazaki, H. Ueda, M. Isobe, Y. Matsushita, and Y. Ueda, J. Phys. Soc. Jpn. **84**, 024718 (2015).
[55] K. Ohwada, T. Yamauchi, Y. Fujii, and Y. Ueda, Phys. Rev. B **85**, 134102 (2012).
[56] M. Tsuchiizu, J. Magn. Magn. Mater. **310**, e200 (2007).
[57] H. Seo, S. Ishibashi, and Y. Otsuka (private communication).
[58] S. Ravy, Chem. Rev. **104**, 5609 (2004).
[59] H. Seo and H. Fukuyama, J. Phys. Soc. Jpn. **67**, 2602 (1998).